# Supplemental Material: Wrinkles, rucks and folds formed in a heavy sheet on a frictional surface

Keisuke Yoshida[1,2*] and Hirofumi Wada[1]
[1] *Department of Physical Sciences, Ritsumeikan University, Kusatsu, Shiga 525-8577, Japan and*
[2] *Research Organization of Science and Technology, Ritsumeikan University, Kusatsu, Shiga 525-8577, Japan*

(Dated: January 1, 2026)

## I. EFFECT OF INDENTER SIZE

To examine the effect of indenter radius on the load–displacement and lifted-radius–displacement relations, we performed finite-element simulations (FES). We chose a circular elastic sheet with $(E, \nu, \rho, h, a, \mu) = (477\ \text{kPa}, 0.47, 1127\ \text{kg/m}^3, 0.27\ \text{mm}, 100\ \text{mm}, 0.31)$, for which $\ell_g = (B/\rho g)^{1/4} \approx 3.1$ mm. Indentation was imposed by gradually increasing a vertical displacement $d$ over a central circular region $0 \le r \le r_{\text{ind}}$. We varied the indenter radius as $r_{\text{ind}} = 0.1$, 0.5, 1, 2, and 5 mm. As shown in Fig. S1, the numerical data approach the point-load predictions in Eqs. (16) and (17) as $r_{\text{ind}}$ decreases. In the moderate deformation regime ($d/h \sim 10^{-1}$), when $r_{\text{ind}} \ll \ell_g (d/h)^{1/4}$, the indentation can be regarded as a concentrated load acting on the sheet. By contrast, for $d/h \gg 1$ the characteristic lifted radius $\ell_g (d/h)^{3/4}$ is typically much larger than $r_{\text{ind}}$ in our setup, so the point-load approximation is well satisfied.

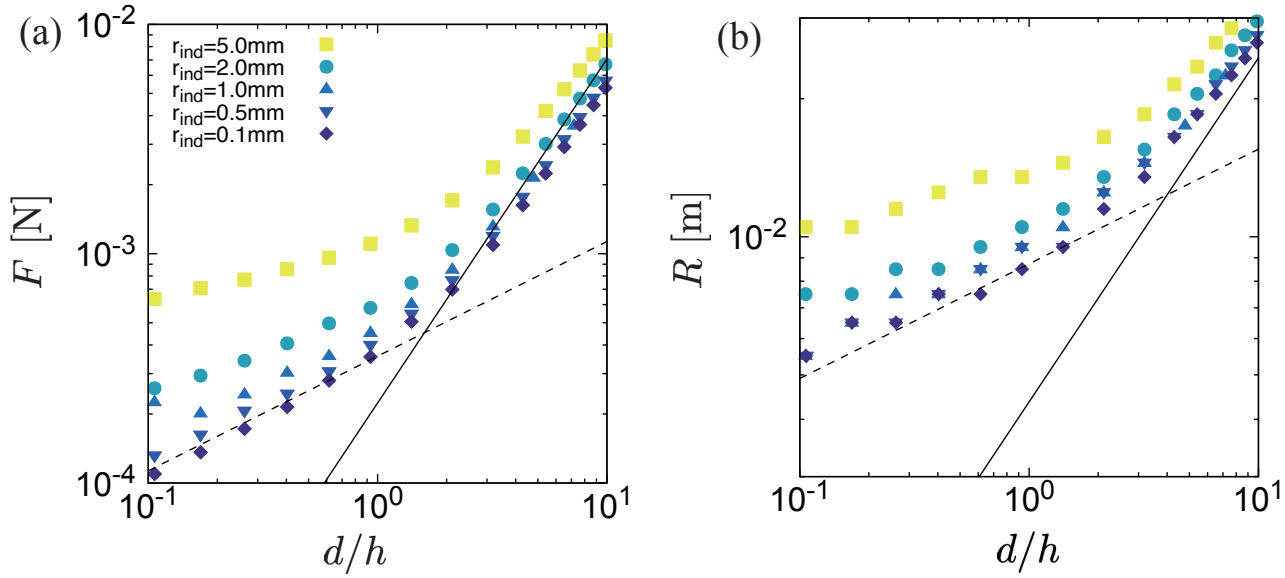


FIG. S1. FES results for varying indenter radii $r_{\text{ind}}$ (all other parameters identical). (a) Load–displacement relation. (b) Lifted radius–displacement relation. The dashed and solid lines represent Eq. (16), (17), (23), and (24) in the main text, which are derived under the point-loading assumption. In both cases, as $r_{\text{ind}}$ decreases, the numerical results approach the theoretical predictions based on the point-load model.

* kyosh424@gmail.com

## II. FULL DERIVATION OF THE MEMBRANE SOLUTIONS

When the indentation height is sufficiently larger than the sheet thickness ($d/h \gg 1$), the equilibrium of a thin membrane subjected to a concentrated load $\mathcal{F}$ is described by the coupled differential equations for the out-of-plane displacement $W(\xi)$ and the Airy stress function $\Psi(\xi)$:

$$-\Psi W' + \frac{\alpha}{2}\xi^2 - \frac{\mathcal{F}}{2\pi} = 0, \tag{S1}$$

$$\xi\frac{d}{d\xi}\left[\frac{1}{\xi}\frac{d}{d\xi}(\xi\Psi)\right] + \frac{1}{2}W'^2 = 0, \tag{S2}$$

where $\xi$ denotes the radial coordinate. The quantities $\xi$, $W$, and $\Psi$ are nondimensionalized according to Eq. (18) in the main text.

Equations (S1) and (S2) with the boundary conditions

$$W(0) = 1,\ W(1) = 0,\ \Psi(0) = 0,\ \Psi'(1) - \nu\Psi(1) = 0, \tag{S3}$$

can be solved analytically in the absence of gravity ($\alpha = 0$) [1]. In particular, for $\nu = 1/3$, the so-called *Schwerin's solution* [2, 3] is given by

$$\Psi^{(0)} = \frac{1}{4}\xi^{1/3}, \tag{S4}$$

$$W^{(0)} = 1 - \xi^{2/3}, \tag{S5}$$

$$\mathcal{F}^{(0)} = \frac{\pi}{3}. \tag{S6}$$

We now consider the case including gravity. The effect of gravity, characterized by the dimensionless parameter $\alpha$ in (S1), is assumed to be small enough to be treated as a perturbation. Expanding $\Psi$, $W$, and $\mathcal{F}$ around the unperturbed solutions:

$$\Psi = \Psi^{(0)} + \alpha\Psi^{(1)} + O(\alpha^2), \tag{S7}$$

$$W = W^{(0)} + \alpha W^{(1)} + O(\alpha^2), \tag{S8}$$

$$\mathcal{F} = \mathcal{F}^{(0)} + \alpha\mathcal{F}^{(1)} + O(\alpha^2). \tag{S9}$$

Solving Eqs. (S1) and (S2) up to $O(\alpha)$ yields

$$W(\xi) = 1 - \xi^{2/3} + \alpha\left(\frac{5}{4}\xi^{8/3} - \frac{1}{4}\xi^{2/3} - \xi^2\right), \tag{S10}$$

$$\Psi(\xi) = \frac{1}{4}\xi^{1/3} + \alpha\left(\frac{1}{2}\xi^{7/3} + \frac{1}{8}\xi^{1/3} - \frac{3}{4}\xi^{5/3}\right), \tag{S11}$$

$$\mathcal{F} = \frac{\pi}{3} + \alpha\frac{\pi}{4}. \tag{S12}$$

The stress components follow from the derivatives of $\Psi$:

$$\Sigma_{rr} \equiv \frac{\Psi}{\xi} = \frac{1}{4}\xi^{-2/3} + \alpha\left(\frac{1}{2}\xi^{4/3} + \frac{1}{8}\xi^{-2/3} - \frac{3}{4}\xi^{2/3}\right), \tag{S13}$$

$$\Sigma_{\theta\theta} \equiv \frac{d\Psi}{d\xi} = \frac{1}{12}\xi^{-2/3} + \alpha\left(\frac{7}{6}\xi^{4/3} + \frac{1}{24}\xi^{-2/3} - \frac{5}{4}\xi^{2/3}\right). \tag{S14}$$

The dimensionless stresses $\Sigma_{\alpha\beta}$ are related to $\sigma_{\alpha\beta}$ through

$$\sigma_{\alpha\beta} = \frac{Ed^2}{R^2}\Sigma_{\alpha\beta}. \tag{S15}$$

To determine the undetermined parameter $\alpha$, we estimate it by minimizing the total energy [3]. First, the stretching

energy is obtained from Eqs. (S10-S14):

$$\mathcal{E}_s = \frac{h}{2}\int_A \sigma_{\alpha\beta}\epsilon_{\alpha\beta} dA \tag{S16}$$

$$= \frac{Ehd^4}{2R^2}\oint d\theta \int_0^1 \xi d\xi \left\{(\Sigma_{rr}+\Sigma_{\theta\theta})^2 - 2(1+\nu)\Sigma_{rr}\Sigma_{\theta\theta}\right\} \tag{S17}$$

$$= \frac{\pi Ehd^4}{R^2}\left\{\frac{5-3\nu}{48} + \alpha\frac{\nu-1/3}{16} + O(\alpha^2)\right\}. \tag{S18}$$

For $\nu = 1/3$, this simplifies to

$$\mathcal{E}_s = \frac{\pi Ehd^4}{R^2}\left\{\frac{1}{12} + O(\alpha^2)\right\}. \tag{S19}$$

The gravitational energy is given by

$$\mathcal{E}_g = \rho g h \int_A w dA \tag{S20}$$

$$= \rho g h R^2 d \oint d\theta \int_0^1 \xi W(\xi) d\xi \tag{S21}$$

$$= 2\pi\rho g h R^2 d\left(\frac{1}{8} - \alpha\frac{17}{224} + O(\alpha^2)\right) \tag{S22}$$

Minimizing $\mathcal{E}_s + \mathcal{E}_g$ with respect to $R$ at the leading order ($O(\alpha^0)$) yields

$$R \approx 3^{-1/4}\left(\frac{E}{\rho g}\right)^{1/4} d^{3/4} \tag{S23}$$

$$= [4(1-\nu^2)]^{1/4}\ell_g\left(\frac{d}{h}\right)^{3/4}. \tag{S24}$$

Comparing Eq. (S24) with Eq. (1) in the main text, we identify

$$c_s = [4(1-\nu^2)]^{1/4} = \left(\frac{32}{9}\right)^{1/4}, \tag{S25}$$

where we have substituted $\nu = 1/3$ in accordance with the above assumption. By definition, once $c_s$ is determined we obtain

$$\alpha = \frac{c_s^4}{12(1-\nu^2)} = \frac{1}{3}. \tag{S26}$$

Using Eq. (S9), the corresponding load becomes $\mathcal{F} \approx 5\pi/12$, and hence

$$F \approx \frac{Ehd^3}{R^2}\mathcal{F} \tag{S27}$$

$$\approx \frac{5\pi(1-\nu^2)}{c_s^2}\rho g h \ell_g^2\left(\frac{d}{h}\right)^{3/2}. \tag{S28}$$

Thus, the prefactor $k_s$ in the scaling laws for the force response $F$ [Eqs. (3) in the main text] is

$$k_s \approx \frac{5\pi}{2}\sqrt{1-\nu^2} = \frac{5\sqrt{2}\pi}{3}. \tag{S29}$$

### A. Rescaling of nondimensional stress

In the main text, the stress distribution is plotted in units of $B/(h\ell_g^2)$, which serves as the characteristic stress scale independent of $d$. Here, we express $\Sigma_{\alpha\beta}$ in terms of $h\ell_g^2\sigma_{\alpha\beta}/B$ by using Eqs. (S15) and (S24):

$$\frac{h\sigma_{\alpha\beta}}{B/\ell_g^2} = \frac{Ehd^2\ell_g^2}{BR^2}\Sigma_{\alpha\beta} \tag{S30}$$

$$= \frac{12(1-\nu^2)}{c_s^2}\left(\frac{d}{h}\right)^{1/2}\Sigma_{\alpha\beta} \tag{S31}$$

$$\approx 4\sqrt{2}\left(\frac{d}{h}\right)^{1/2}\Sigma_{\alpha\beta}. \tag{S32}$$

## III. ESTIMATION OF THE STICK–SLIDE BOUNDARY

We focus on the planar region of the sheet ($R < r < a$). A frictional force per unit area, $\boldsymbol{f}(r,\theta) = f_r\hat{\boldsymbol{e}}_r + f_\theta\hat{\boldsymbol{e}}_\theta$ acts between the sheet and the substrate. As the indentation height $d$ is gradually increased, the in-plane stress in the sheet may locally exceed the maximum static friction, so that regions of sticking and sliding can coexist.

Here we consider the case in which $R < r < r_*$ is the sliding region, while $r_* < r < a$ corresponds to the sticking region. For $r \gg r_*$, the traction remains smaller than the maximum static friction, so material points stay pinned to the substrate. As $r$ decreases toward $r_*$, the tensile stress increases, and for $r < r_*$ material points undergo stick–slip motion.

We consider the force balance in an infinitesimal domain $d\Omega \equiv [r, r+dr]\times[\theta, \theta+d\theta]$, where $\times$ denotes the Cartesian product:

$$\frac{1}{r}\frac{\partial}{\partial r}(rh\sigma\hat{\boldsymbol{e}}_r) + \frac{1}{r}\frac{\partial}{\partial\theta}(h\sigma\hat{\boldsymbol{e}}_\theta) + \boldsymbol{f} = \boldsymbol{0}, \tag{S33}$$

where the stress tensor is expressed as $\sigma = \sigma_{\alpha\beta}\hat{\boldsymbol{e}}_\alpha \otimes \hat{\boldsymbol{e}}_\beta$, with $\otimes$ indicating the tensor product. For axisymmetric states, this equation reduces to the classical Lamé-type equilibrium equation [4]:

$$\frac{\sigma_{rr}-\sigma_{\theta\theta}}{r} + \frac{d}{dr}\sigma_{rr} + \frac{f_r}{h} = 0. \tag{S34}$$

We consider the case in which the boundary $r = r_*$ lies within the infinitesimal domain $d\Omega$. Using the maximum static friction at this boundary,

$$f_r(r_*) = \mu\rho g h, \tag{S35}$$

together with the overall force balance, we estimate the relationship between $d$ and $r_*$ as follows. In the planar region, the stresses decay as $\sigma_{rr}(r) \sim \sigma_{rr}(R)R^2/r^2$ and $\sigma_{\theta\theta}(r) \sim -\sigma_{rr}(R)R^2/r^2$. Using $\sigma_{rr}(R) \sim E(d/R)^2$ and Eq. (S34), and balancing the terms in Eq. (S34) at $r \sim r_*$, we obtain the scaling relation

$$r_* \sim \left(\frac{E}{\mu\rho g}\right)^{1/3} d^{2/3}. \tag{S36}$$

This scaling suggests that, in the absence of friction ($\mu = 0$), the stick–slip boundary $r_*$ diverges, so that the entire contact region slips for arbitrarily small indentation, consistent with physical intuition. Furthermore, by setting $r_* = a$ in Eq. (S36), we can estimate the critical indentation height $d_*$ at which the entire contact region begins to slide:

$$d_* \sim \left(\frac{\mu\rho g}{E}\right)^{1/2} a^{3/2}. \tag{S37}$$

We compare Eq. (S36) with the numerical results. In our finite-element simulations (FES), we define "substantial slip" by the criterion $|u_r(r)| > \varepsilon\Delta x$, where $\Delta x$ is the typical mesh size and $\varepsilon = 10^{-3}$ (See also §V in the main text). Using the parameter set as in Table II of the main text, we examined the azimuthally averaged radial displacement $\overline{u_r}(r) \equiv \frac{1}{2\pi}\oint u_r(r,\theta)d\theta$ over the entire contact region $R < r < a$. We then identified the location $r_*$ separating regions

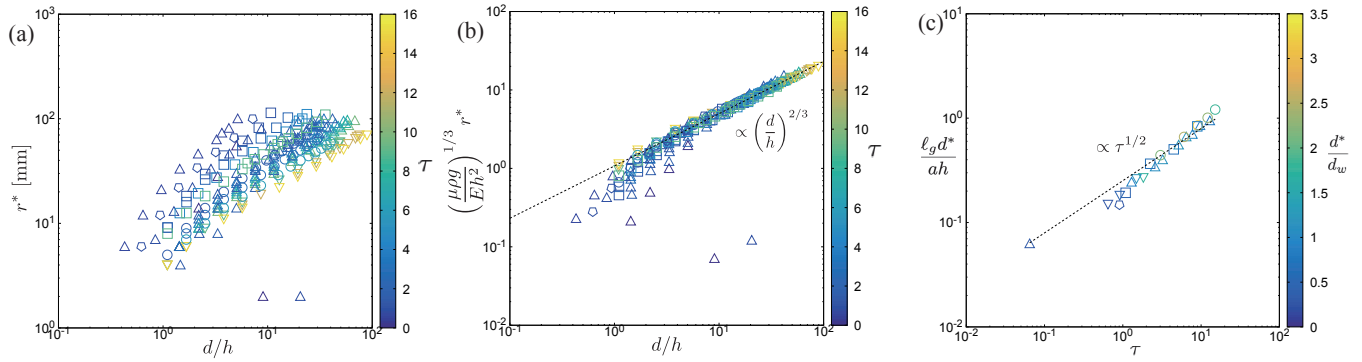


FIG. S2. Finite element simulation data on frictional slip in the contact region. (a) Relationship between the stick-slide boundary $r_*$ and indentation height $d$. The color bar indicates the frictional strength $\tau$. (b) Same data as in (a) but rescaled according to Eq. (S38); the dashed line represents Eq. (S38). (c) Critical indentation height $d_*$ at which the stick–slip boundary reaches the outer edge ($r_* = a$), as a function of $\tau$. The dashed line shows Eq. (S39). The color bar represents the ratio $d_*/d_w$, where $d_w$ is the critical displacement at the onset of wrinkling.

with substantial slip from those where the displacement remains below the threshold, $|u_r(r)| < \varepsilon\Delta x$. The results are shown in Figs. S2 (a) and (b), where the dashed line represents

$$\left(\frac{\mu\rho g}{Eh^2}\right)^{1/3} r_* \approx 1.07 \left(\frac{d}{h}\right)^{2/3}, \tag{S38}$$

with the prefactor 1.07 determined from a fit to the FES results.

We also measured the critical displacement $d_*$ at which the outer edge of the sheet ($r = a$) begins to slip in our FES. Equation (S37) can be rewritten in terms of the relative frictional stress $\tau$ (see Eq. (32) in the main text) as $\ell_g d_*/(ah) \sim \tau^{1/2}$. Our numerical results, shown in Fig. S2 (c), are consistent with this scaling. By fitting the numerical data, we obtain the best-fit prefactor

$$\frac{\ell_g d_*}{ah} \approx 0.23\ \tau^{1/2}. \tag{S39}$$

The color bar in Fig. S2 (c) represents the ratio $d_*/d_w$ measured in these FESs. For $\tau \lesssim 1$, $d_*/d_w$ tends to less than unity. This trend is consistent with the assumption used in the main text that "complete slip" occurs prior to the onset of wrinkling.

## IV. PLANE STRESS UNDER THE QUASI-STATIC SLIDING

Here, we derive the stress field in the contact region after complete slipping has occurred. This analysis allows us to clarify how friction affects the stress distribution relevant to the onset of wrinkling (see § VI in the main text).

As in the main text, we focus on the quasi-static indentation and idealize the sheet–substrate interface as being everywhere close to the Coulomb threshold, i.e. $f_t = \mu f_n$. In this effective description, the frictional force is taken to have an approximately uniform magnitude $f_r \approx \mu\rho g h$ over the entire contact region. Under this assumption, we solve the following differential equation:

$$\frac{\sigma_{rr} - \sigma_{\theta\theta}}{r} + \frac{d}{dr}\sigma_{rr} + \mu\rho g = 0. \tag{S40}$$

The sheet edge at $r = a$ is stress-free, while a finite tension $T$ is applied at $r = R$. Accordingly, the boundary conditions are

$$\sigma_{rr}(R) = T, \tag{S41}$$
$$\sigma_{rr}(a) = 0. \tag{S42}$$

Hereafter, we explicitly denote the frictional dependence of the stress by writing $\sigma_{\alpha\beta}(r;\mu)$; for example, $\sigma_{\alpha\beta}(r;0)$ corresponds to the frictionless case.

We first consider the case of $\mu = 0$. The solution is

$$\sigma_{rr}(r;0) = \frac{T}{1-(R/a)^2}\left\{\left(\frac{R}{r}\right)^2 - \left(\frac{R}{a}\right)^2\right\} \sim T\frac{R^2}{r^2}, \tag{S43}$$

$$\sigma_{\theta\theta}(r;0) = -\frac{T}{1-(R/a)^2}\left\{\left(\frac{R}{r}\right)^2 + \left(\frac{R}{a}\right)^2\right\} \sim -T\frac{R^2}{r^2}. \tag{S44}$$

Here, the symbol "$\sim$" indicates an approximation valid near $r \sim R$ under the assumption that the sheet radius is sufficiently large, i.e., $R \ll a$.

For $\mu > 0$, additional terms proportional to the friction coefficient $\mu$ are superimposed on $\sigma_{\alpha\beta}(r;0)$, as follows:

$$\sigma_{rr}(r;\mu) = \sigma_{rr}(r;0) + \frac{2+\nu}{3}\mu\rho g a\left\{1 - \frac{r}{a} - \frac{(R/r)^2-(R/a)^2}{1+R/a}\right\}, \tag{S45}$$

$$\sigma_{\theta\theta}(r;\mu) = \sigma_{\theta\theta}(r;0) + \frac{2+\nu}{3}\mu\rho g a\left\{1 - \frac{1+2\nu}{2+\nu}\frac{r}{a} + \frac{(R/r)^2+(R/a)^2}{1+R/a}\right\}. \tag{S46}$$

The onset of wrinkling is governed by the stresses near $r \sim R$. For a sufficiently large sheet, i.e., under the assumption $R \ll a$, the hoop stress at $r = R$ is obtained as

$$\sigma_{\theta\theta}(R;\mu) = -T\left\{1 + O((R/a)^2)\right\} + \frac{2+\nu}{3}\mu\rho g a\left\{2 - \frac{3(1+\nu)}{2+\nu}\frac{R}{a} + O((R/a)^2)\right\}. \tag{S47}$$

The parameter $T$ should, in principle, be determined by the matching the solution in the lifted region for $r < R$, obtained from the FvK equations, to the outer planar solution given by Eqs. (S45) and (S46). Such a matching problem is left for future work. Instead, in the following subsection we use FESs to assess how $T$ depends on the friction coefficient $\mu$.

### A. Frictional dependence of the boundary tension $T$

To examine the $\mu$-dependence of $T$ numerically, we analyzed the stress profiles in the planar region using FES and fitted them to Eq. (S45) treating $T$ as a fitting parameter. The results for models with identical material and geometric parameters but different friction coefficients, $\mu$, are shown in Fig. S3. Each fitting was performed for the stress field at the indentation height corresponding to $d \approx d_w^0$. As shown in Fig. S3(b), the fitted values of $T$ increase sublinearly with $\mu$ from the value at $\mu = 0$ (denoted by $T_0$). Since the purpose of this section is to provide an order-of-magnitude estimation based on Eq. (S47), a detailed theoretical analysis of the $\mu$-dependence of $T$ is left for future work. Combining these numerical results with Eq. (S45), we find that the radial stress $\sigma_{rr}(r)$ exhibits only a weak dependence on $\mu$ near $r \sim R$ for small $\tau$. By contrast, the hoop stress $\sigma_{\theta\theta}(r)$ contains a term proportional to $\mu\rho g a$ as shown in Eq. (S47). This result justifies the assumption made in deriving Eqs. (34) and (35) in the main text: that $\sigma_{rr}(R)$ depends only weakly on $\tau$, whereas $\sigma_{\theta\theta}(R)$ exhibits a first-order dependence on $\tau$, at least for small $\tau$.


[1] D. Vella and B. Davidovitch, Indentation metrology of clamped, ultra-thin elastic sheets, Soft Matter **13**, 2264 (2017).
[2] E. H. Mansfield, *The bending and stretching of plates*, 2nd ed. (Cambridge University Press, 1989).
[3] J. Chopin, D. Vella, and A. Boudaoud, The liquid blister test, Proc. R. Soc. A: Math. Phys. Eng. Sci. **464**, 2887 (2008).
[4] S. Timoshenko and J. Goodier, *Theory of Elasticity*, Engineering mechanics series (McGraw-Hill, 1969).

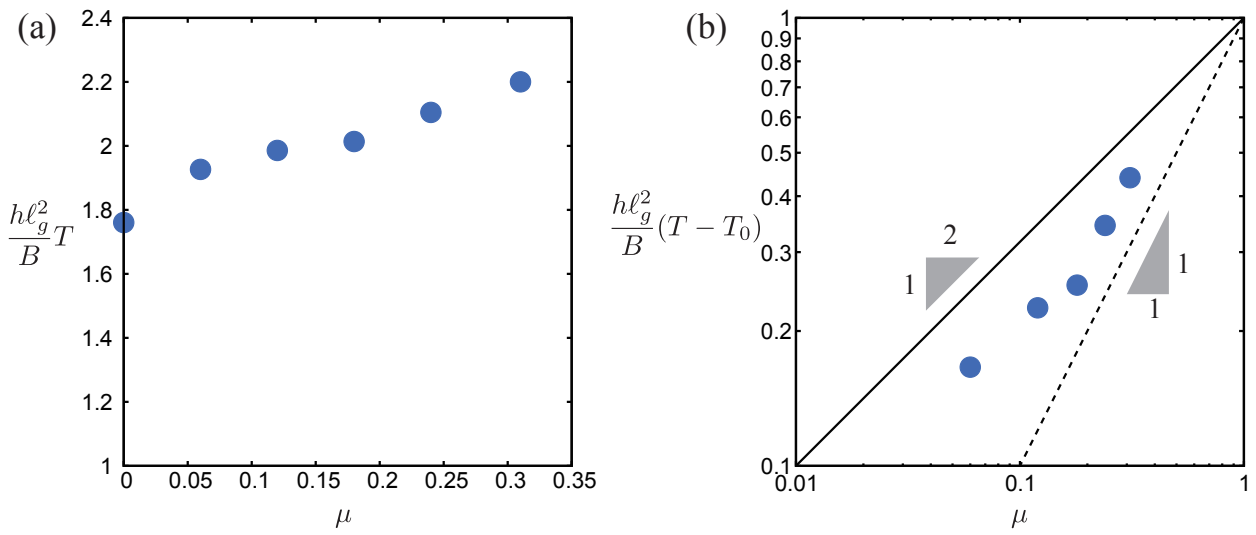


FIG. S3. Relationship between $T \equiv \sigma_{rr}(R)$ and the static friction coefficient $\mu$ obtained from FES. The elastic sheet parameters are $(E, \nu, \rho, h, a) = (477\ \text{kPa},\ 0.47,\ 1127\ \text{kg/m}^3,\ 0.27\ \text{mm}, 100\ \text{mm})$. The value of $T$ was determined by fitting the azimuthally averaged radial stress $\overline{\sigma_{rr}}(r)$ at $d \approx d_w^0$ to Eqs. (S43) and (S45). (a) Dimensionless $T$ as a function of $\mu$. (b) The difference $T - T_0$ versus $\mu$, where $T_0$ denotes the value of $T$ at $\mu = 0$. The solid and dashed lines show reference curves proportional to $\mu^{1/2}$ and $\mu$, respectively.